

Article

Effects of Magnetic Fields, Coupled Stefan Blowing and Thermodiffusion on Ferrofluid Transport Phenomena

Rohana Abdul Hamid ^{1,2}, Roslinda Nazar ^{3,*}, Kohilavani Naganthran ^{4,5,*}  and Ioan Pop ⁶

¹ Centre of Excellence for Social Innovation & Sustainability (CoESIS), Universiti Malaysia Perlis, Arau 02600, Malaysia; rohanahamid@unimap.edu.my

² Boundary Layer Research Group, Institute of Engineering Mathematics, Faculty of Applied and Human Sciences, Universiti Malaysia Perlis, Arau 02600, Malaysia

³ Department of Mathematical Sciences, Faculty of Science and Technology, Universiti Kebangsaan Malaysia, Bangi 43600, Malaysia

⁴ Institute of Mathematical Sciences, Faculty of Science, Universiti Malaya, Kuala Lumpur 50603, Malaysia

⁵ Center for Data Analytics, Consultancy and Services, Faculty of Science, Universiti Malaya, Kuala Lumpur 50603, Malaysia

⁶ Department of Mathematics, Babeş-Bolyai University, 400084 Cluj-Napoca, Romania; ipop@math.ubbcluj.ro

* Correspondence: rnm@ukm.edu.my (R.N.); kohl@um.edu.my (K.N.)

Abstract: The paramagnetic feature of ferrofluid allows it to be utilised in electronic devices and improvise fluid circulation in transformer windings. Hence, the present article aims to conduct the numerical study of ferrofluid boundary layer flow along with the Stefan blowing, velocity and thermal slip, and Soret effects within the stagnation region over a stretching/shrinking surface. The governing equations were solved numerically using the `bvp4c` function in the MATLAB computing package. Based on the results, a stronger magnetic field of ferrofluid was needed to identify the numerical solutions past the shrinking surface, while the Stefan blowing diminished the solution's availability. More than one solution is acquired for some specific values of the shrinking parameter, and the stability analysis validated that only one solution is reliable and stable.

Keywords: ferrofluidslip effect; Stefan blowing; thermodiffusion

MSC: 34B15; 76Dxx



Citation: Hamid, R.A.; Nazar, R.; Naganthran, K.; Pop, I. Effects of Magnetic Fields, Coupled Stefan Blowing and Thermodiffusion on Ferrofluid Transport Phenomena. *Mathematics* **2022**, *10*, 1646. <https://doi.org/10.3390/math10101646>

Academic Editors: Camelia Petrescu and Valeriu David

Received: 12 March 2022

Accepted: 9 May 2022

Published: 12 May 2022

Publisher's Note: MDPI stays neutral with regard to jurisdictional claims in published maps and institutional affiliations.



Copyright: © 2022 by the authors. Licensee MDPI, Basel, Switzerland. This article is an open access article distributed under the terms and conditions of the Creative Commons Attribution (CC BY) license (<https://creativecommons.org/licenses/by/4.0/>).

1. Introduction

The evaporation process is very beneficial in industries that require the removal of unwanted fluids, such as the food industry. To mention a few, evaporation is applied to concentrate milk, fruit juice, jams, jellies, and sugar solutions for crystallisation [1]. Furthermore, evaporation is crucial in the pulp and paper industry, where it is used in the drying section, which is the final and the most vital section to produce paper [2]. In a particular circumstance, the species transfer or mass transfer in evaporation can create a different fluid motion. The movement of the species from the interface to the free stream is called the blowing effect or the Stefan blowing effect because the concept originates from the Stefan problem of the mass transfer [3]. The formulations of the mass transfer are similar to the heat transfer equation, but in this problem, the present investigation involves the coupled blowing effect. Moreover, Fang and Jing [3], who introduced the influence of coupled Stefan blowing induced by species transport, suggested that the momentum and the concentration equations should be coupled because the species transfer and the flow field depend on each other. Then, Fang [4] revisited the work in [3] to examine the transport phenomena from the view of unsteady stagnation-point flow and solved analytically in terms of an incomplete Gamma function. After that, the coupled Stefan blowing impact has been considered in the boundary layer models under various settings and external forces,

for instance, in the bioconvection flow [5], magnetohydrodynamics [6], and anisotropic slip [7].

Since very few studies can be found regarding the Stefan blowing effect, we are interested in studying this problem with the addition of the Soret effect (or thermodiffusion), velocity slip, and thermal slip over a stretching or shrinking sheet in a ferrofluid. It is assumed in the present study that the movement of the species particles that is saturated at the surface results from the temperature gradient. This phenomenon is called thermophoresis or the Soret effect and has been studied by Ryskin and Pleiner [8], Ramreddy et al. [9], and Pal et al. [10] in nanofluids, while Arif et al. [11] studied it in a hybrid nanofluid. Furthermore, the study of the slip effect is necessary because the presence of the species blowing at the interface might contribute to the wall slip where the fluid velocity and temperature at the surface are not zero. It was also explained by Uddin et al. [12] that boundary slip occurs in a fluid that contains particulates, such as emulsions and suspensions. Hence, they studied the effects of the slip and the Stefan blowing in a nanofluid that contains gyrotactic microorganisms. On the other hand, many other researchers also considered the slip effect in their shrinking sheet problem, such as Singh and Chamkha [13], who reported the numerical analysis on the effects of the second-order slip on a permeable, vertical isothermal shrinking sheet. In addition, Mahapatra and Nandy [14], Aman et al. [15], and Merkin et al. [16] investigated the flow induced by the shrinking sheet with the slip effect near a stagnation point and obtained non-uniqueness solutions. This is in accordance with the result reported by [17], where the existence of the similarity solutions is guaranteed within the stagnation region past the shrinking surfaces.

On the other hand, we also aim to study the effect of the Stefan blowing in a ferrofluid that contains magnetite nanoparticles (Fe_3O_4). Apart from the nanofluids, which consider different types of nanoparticles as was examined by the theoretical works in [18–21], ferrofluid has become one of the essential fields of interest. Ferrofluid has properties that can be controlled and can absorb electromagnetic energy to increase heat when the external magnetic field is applied. Hence, ferrofluid is beneficial in many applications, such as biomedicine, solar system design, and technological applications, for example, dynamic sealing, damping, and doping of specialised materials [22]. Shokrollahi [23] identified that ferrofluid had been used in the mechanism for the early detection of cancer, as the contrast agent for the Magnetic Resonance Imaging (MRI), and in the development of an implantable artificial heart. In this problem, ferrofluid is numerically modelled using a single-phase approach. Henceforth, the base fluid and the magnetic nanoparticles are assumed in thermal equilibrium concerning their physical properties and moving with the same velocity. Ryskin et al. [24] described that most experiments on ferrofluids could be conducted as a single-phase model because the Lewis number of the ferrofluid is minimal. Several numerical studies of the ferrofluid used the single-phase model [25–28]. Recently, Hamid et al. [29] scrutinised the impact of viscous dissipation on dusty ferrofluid flow and heat transfer over a shrinking flat surface (single-phase model) and showed that the shear stress increases when the dust particles augment in the ferrofluid.

Acknowledging these valuable theoretical works reported within the scope of the magnetic field, ferrofluid flow, coupled Stefan blowing, and Soret impact, it was found that there is a research gap where the influences of the magnetic field, Soret coefficient, velocity slip, and thermal slip have not been examined on the ferrofluid flow past the moving surface. The numerical outputs are generated as the intensity of the external forces varies. More than one solution that elucidates the transport phenomena is identified, and stability analysis is implemented to justify the solution's stability. The present valuable work has significance in hydrometallurgical applications.

2. Mathematical Model

We examined a steady, two-dimensional, laminar, stagnation-point flow of a viscous and incompressible water-based ferrofluid with the velocity and thermal slips as shown in Figure 1, where x and y are the Cartesian coordinates considered past the moving

surface where the sheet moves in a manner of either stretching or shrinking, and normal to it, respectively. The sheet moves with a velocity defined as $u = \lambda U_w + U_{slip}$, where U_w and U_{slip} are the sheet velocity and slip velocity, respectively, and λ is the parameter that measures the stretching or shrinking rate. The free stream velocity is denoted by U_e . Meanwhile, the ferrofluid temperature, T at the surface is denoted as T_w . A transverse magnetic field was assumed to exist in the manner of normal to the surface where B_0 is the magnetic field strength. Additionally, it was assumed that no external electric field is available, and the electric field caused by the polarisation charges are omitted. We took that a binary fluid saturates the surface with dissolved species and magnetite ferroparticles (Fe_3O_4) in this problem. It was also assumed that the species' massive mass transfer occurred with velocity during the stretching/shrinking action $V_w(x)$ and generated a blowing effect [3]. It should be noted that the species does not interact with the magnetite nanoparticles.

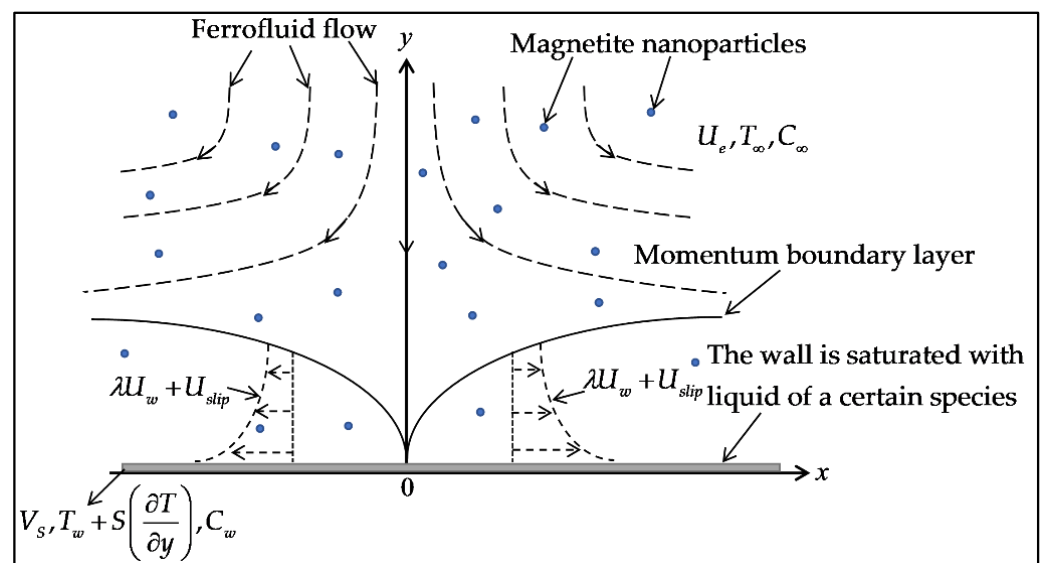


Figure 1. Present flow problem's physical model.

Based on these assumptions, the following mathematical model can be formulated [30]:

$$\frac{\partial u}{\partial x} + \frac{\partial v}{\partial y} = 0, \tag{1}$$

$$u \frac{\partial u}{\partial x} + v \frac{\partial u}{\partial y} = U_e \frac{dU_e}{dx} + \nu_{ff} \frac{\partial^2 u}{\partial y^2} - \frac{\sigma_{ff} B_0^2}{\rho_{ff}} (u - U_e), \tag{2}$$

$$u \frac{\partial T}{\partial x} + v \frac{\partial T}{\partial y} = \alpha_{ff} \frac{\partial^2 T}{\partial y^2}, \tag{3}$$

$$u \frac{\partial C}{\partial x} + v \frac{\partial C}{\partial y} = D_S \frac{\partial^2 C}{\partial y^2} + D_{CT} \frac{\partial^2 T}{\partial y^2}, \tag{4}$$

where u and v are the velocity components along with the directions x and y , respectively; ν_{ff} is the ferrofluid kinematic viscosity; σ_{ff} is the ferrofluid electrical conductivity; ρ_{ff} is the ferrofluid density; T is the temperature; α_{ff} is the ferrofluid thermal diffusivity; C is the species concentration; D_S is the species diffusivity; and D_{CT} is the Soret-type diffusivity. The boundary conditions at the sheet are ([15,31]):

$$\begin{aligned}
 u &= \lambda U_w + U_{slip} = \lambda cx + L \left(\frac{\partial u}{\partial y} \right), v = V_S = k(x) \frac{\partial C}{\partial y}, T = T_w + S \left(\frac{\partial T}{\partial y} \right), \\
 C &= C_w \text{ at } y = 0, \\
 u &\rightarrow U_e(x) = ax, T \rightarrow T_\infty, C \rightarrow C_\infty \text{ as } y \rightarrow \infty,
 \end{aligned}
 \tag{5}$$

where λ is the stretching parameter ($\lambda > 0$) or the shrinking parameter ($\lambda < 0$), a, c are the positive constants, L is the velocity slip parameter, S is the thermal slip parameter, and $k(x)$ signifies the blowing function. The effective properties of ferrofluid (subscript ff) may be conveyed in terms of the base fluid’s properties (subscript f) and solid ferroparticles (subscript s) and the solid ferroparticles’ volume fraction, ϕ , as follows [32]:

$$\begin{aligned}
 \nu_{ff} &= \frac{\mu_{ff}}{\rho_{ff}}, \mu_{ff} = \frac{\mu_f}{(1-\phi)^{2.5}}, \rho_{ff} = (1-\phi)\rho_f + \phi\rho_s, \\
 \alpha_{ff} &= \frac{k_{ff}}{(\rho c_p)_{ff}}, (\rho c_p)_{ff} = (1-\phi)(\rho c_p)_f + \phi(\rho c_p)_s, \\
 \frac{k_{ff}}{k_f} &= \frac{k_s + 2k_f - 2\phi(k_f - k_s)}{k_s + 2k_f + \phi(k_f - k_s)}, \frac{\sigma_{ff}}{\sigma_f} = 1 + \frac{3 \left(\frac{\sigma_s}{\sigma_f} - 1 \right) \phi}{\left(\frac{\sigma_s}{\sigma_f} + 2 \right) - \left(\frac{\sigma_s}{\sigma_f} - 1 \right) \phi}.
 \end{aligned}
 \tag{6}$$

We then introduced the following similarity variables as [30]:

$$\begin{aligned}
 u &= cx f'(\eta), v = -\sqrt{c\nu_{ff}} f(\eta), \eta = \sqrt{c/\nu_{ff}} y \\
 \theta(\eta) &= \frac{T - T_\infty}{T_w - T_\infty}, H(\eta) = \frac{C - C_\infty}{C_w - C_\infty}.
 \end{aligned}
 \tag{7}$$

Furthermore, it is a necessity for $f(0)$ to be independent of x , if and only if $k(x)$ and x vary inversely or $k(x) \propto \frac{1}{x}$ [31]. Eventually, the blowing function can be written in the following form: $k(x) = \frac{-\kappa\nu_f}{C_w - C_\infty}$, where the nondimensional blowing parameter κ is fixed to be within the range of $\kappa \geq 0$ to allow the model to be transformed into a similarity form. Substituting (7) into Equations (1)–(4) and boundary conditions (5) yielded the following simplified mathematical model,

$$\varepsilon_1 f''' + f f'' - f'^2 - \varepsilon_2 M(f' - A) + A^2 = 0,
 \tag{8}$$

$$\varepsilon_3 \theta'' + \text{Pr} f \theta' = 0,
 \tag{9}$$

$$H'' + Sc f H' + S_T Sc \theta'' = 0,
 \tag{10}$$

with the boundary condition:

$$\begin{aligned}
 f(0) &= \kappa H'(0), f'(0) = \lambda + \delta f''(0), \theta(0) = 1 + \delta_T \theta'(0), H(0) = 1, \\
 f'(\eta) &\rightarrow A, \theta(\eta) \rightarrow 0, H(\eta) \rightarrow 0 \text{ as } \eta \rightarrow \infty,
 \end{aligned}
 \tag{11}$$

where

$$\begin{aligned}
 \varepsilon_1 &= \frac{\nu_{ff}}{\nu_f} = \frac{1}{(1-\phi)^{2.5}((1-\phi) + \phi(\rho_s/\rho_f))}, \varepsilon_2 = \frac{\sigma_{ff}/\sigma_f}{(1-\phi) + \phi(\rho_s/\rho_f)}, \\
 \varepsilon_3 &= \text{Pr} \frac{\alpha_{ff}}{\nu_f} = \text{Pr} \frac{k_{ff}/k_f}{\left(1 - \phi + \phi \frac{(\rho c_p)_s}{(\rho c_p)_f} \right)}.
 \end{aligned}
 \tag{12}$$

The other parameters are the velocity ratio A , the magnetic interaction parameter M , the Prandtl number Pr , the Schmidt number Sc , the Soret parameter S_T , the blowing parameter κ , the velocity slip parameter δ , and the thermal slip parameter δ_T , which are defined as:

$$A = \frac{a}{c}, M = \frac{\sigma_f B_0^2}{a \rho_f}, Pr = \frac{\nu_f}{\alpha_f}, Sc = \frac{\nu_f}{D_s},$$

$$S_T = \frac{D_{CT}(T_w - T_\infty)}{\nu_f(C_w - C_\infty)}, \delta = L \sqrt{\frac{c}{\nu_f}}, \delta_T = S \sqrt{\frac{c}{\nu_f}}. \tag{13}$$

The physical quantities that are important in the present work are the skin friction coefficient C_f and the local Nusselt number Nu_x , which are expressed as

$$C_f = \frac{\tau_w}{\rho_f U_w^2(x)}, Nu_x = \frac{x q_w}{k_f(T_w - T_\infty)}, \tag{14}$$

The shear stress τ_w and the surface heat flux q_w are given by

$$\tau_w = \mu_{ff} \left(\frac{\partial u}{\partial y} \right)_{y=0}, q_w = -k_{ff} \left(\frac{\partial T}{\partial y} \right)_{y=0}, \tag{15}$$

Hence, the dimensionless wall shear stress $C_f Re_x^{1/2}$ and the dimensionless heat flux $Nu_x Re_x^{-1/2}$ are defined as

$$C_f Re_x^{1/2} = \frac{f''(0)}{(1 - \phi)^{2.5}}, Nu_x Re_x^{-1/2} = -\frac{k_{ff} \theta'(0)}{k_f}, \tag{16}$$

where $Re_x = U_w(x)x/\nu_f$.

3. Stability Analysis

The stability analysis is started by introducing the non-dimensional time variable or τ as shown below

$$u = cx f'(\eta, \tau), v = -\sqrt{c\nu_f} f(\eta, \tau), \eta = \sqrt{c/\nu_f} y, \tau = ct,$$

$$\theta(\eta, \tau) = \frac{T - T_\infty}{T_w - T_\infty}, H(\eta, \tau) = \frac{C - C_\infty}{C_w - C_\infty}. \tag{17}$$

Next, using (17), Equations (1)–(4) become the unsteady equations as follows:

$$\varepsilon_1 \frac{\partial^3 f}{\partial \eta^3} + f \frac{\partial^2 f}{\partial \eta^2} - \left(\frac{\partial f}{\partial \eta} \right)^2 - \varepsilon_2 M \left(\frac{\partial f}{\partial \eta} - A \right) + A^2 - \frac{\partial^2 f}{\partial \eta \partial \tau} = 0, \tag{18}$$

$$\frac{\varepsilon_3}{Pr} \frac{\partial^2 \theta}{\partial \eta^2} + f \frac{\partial \theta}{\partial \eta} - \frac{\partial \theta}{\partial \tau} = 0, \tag{19}$$

$$\frac{\partial^2 H}{\partial \eta^2} + Sc f \frac{\partial H}{\partial \eta} + Sc S_T \frac{\partial^2 \theta}{\partial \eta^2} - \frac{\partial H}{\partial \tau} = 0, \tag{20}$$

with the boundary conditions:

$$f(0, \tau) = \kappa \frac{\partial H(0, \tau)}{\partial \eta}, \frac{\partial f(0, \tau)}{\partial \eta} = \lambda + \delta \frac{\partial^2 f(0, \tau)}{\partial \eta^2}, \theta(0, \tau) = 1 + \delta_T \frac{\partial \theta(0, \tau)}{\partial \eta}, H(0, \tau) = 1,$$

$$\frac{\partial f(\eta, \tau)}{\partial \eta} \rightarrow A, \theta(\eta, \tau) \rightarrow 0, H(\eta, \tau) \rightarrow 0 \text{ as } \eta \rightarrow \infty. \tag{21}$$

Then, the linear stability of the solutions is determined by using the following:

$$f(\eta, \tau) = f_0(\eta) + e^{-\gamma \tau} J(\eta), \theta(\eta, \tau) = \theta_0(\eta) + e^{-\gamma \tau} Q(\eta),$$

$$H(\eta, \tau) = H_0(\eta) + e^{-\gamma \tau} B(\eta), \tag{22}$$

where $f_0(\eta)$, $\theta_0(\eta)$, and $H_0(\eta)$ indicate the steady solution of the Equations (8)–(10). Further, $J(\eta)$, $Q(\eta)$, and $B(\eta)$ are assumed to be small relative to $f_0(\eta)$, $\theta_0(\eta)$, and $H_0(\eta)$ so the disturbances are minimal [33]. Additionally, γ is the unknown eigenvalue and portrays the disturbance’s growth (or decay) rate. Using (22) in (18)–(20) and setting $J(\eta) = J_0(\eta)$, $Q(\eta) = Q_0(\eta)$, and $B(\eta) = B_0(\eta)$ to test the steady flow solutions’ stability, we obtain the following eigenvalues equations:

$$\epsilon_1 J_0''' + f_0 J_0'' + f_0' J_0 - 2f_0' J_0' - \epsilon_2 M J_0' + \gamma J_0' = 0, \tag{23}$$

$$\frac{\epsilon_3}{Pr} Q_0'' + f_0 Q_0' + J_0 \theta_0' + \gamma Q_0 = 0, \tag{24}$$

$$B_0'' + Sc(f_0 B_0' + J_0 H_0') + S_T Sc Q_0'' + \gamma B_0 = 0, \tag{25}$$

and the boundary conditions become:

$$\begin{aligned} J_0(0) &= \kappa B_0'(0), J_0'(0) = \delta J_0''(0), Q_0(0) = \delta_T Q_0'(0), B_0(0) = 0, \\ J_0'(\eta) &\rightarrow 0, Q_0(\eta) \rightarrow 0, B_0(\eta) \rightarrow 0 \text{ as } \eta \rightarrow \infty. \end{aligned} \tag{26}$$

The range of possible eigenvalues γ in the Equations (23)–(25) can be obtained by resting either one of the outer boundary conditions of $J_0(\eta)$, $Q_0(\eta)$, or $B_0(\eta)$ [34]. This procedure is a must in executing the stability analysis because it is required only that the solution should not be exponentially large as τ approaches ∞ . Thus, it is necessary to hold $J_0'(\infty) \rightarrow 0$ and replace it with a new boundary condition $J_0''(0) = 1$. Moreover, since any constant multiple of $J_0(\eta)$ is also considered a solution, $J_0''(0) = 1$ can be fixed without the loss of generality to solve Equations (23)–(25) as an initial value problem. This problem then can be solved via the `bvp4c` function to distinguish the stable and unstable solutions.

4. Results and Discussion

This section presents and discusses the numerical outputs generated via the `bvp4c` function. The thermophysical properties values of the magnetite ferroparticles given in Table 1 were utilised.

Table 1. Values of the physical properties ([25,35]).

Physical Properties	ρ (kg/m ³)	C_p (J/KgK)	k (W/mK)	σ (Ωm) ^{−1}
Base fluid	997.1	4179	0.613	0.05
Ferroparticle	5180	670	9.7	25,000

We also compared the previous work by Mahapatra and Gupta [36] and Khan et al. [30], as shown in Tables 2 and 3. It is apparent from these tables that the present study agrees relatively well with the previous works in the literature. Unless otherwise stated, the values for the parameters were chosen as the following: $\phi = 0.01$, $M = 1$, $A = 1$, $Pr = 6.2$, $Sc = 0.66$, $\kappa = 1$, $S_T = 1$, $\delta = 1$, and $\delta_T = 1$. The values of the Stefan blowing parameter κ were chosen to be positive because we considered the effects of the species blowing to the ambient.

Table 2. Comparison of $C_f Re_x^{1/2}$ for pure water.

A	[36]	[30]	Present Values
0.1	−0.9694	−0.96938	−0.969386
0.2	−0.9181	−0.91810	−0.918107
0.5	−0.6673	−0.66726	−0.667264
2	2.0175	2.01750	2.017503
3	4.7293	4.72928	4.729282

Table 3. Comparison of $-C_f Re_x^{1/2}$ for a water-based ferrofluid (Fe_3O_4) with the variation of M , ϕ and A .

Parameters			[30]	Present Values
M	ϕ	A		
0	0.01	0	1.03366	1.033668
		0.3	0.87801	0.878017
		0.5	0.66726	0.689728
	0.1	0	1.35914	1.359170
		0.3	1.15448	1.154506
		0.5	0.90690	0.906924
1	0.01	0	1.44703	1.447035
		0.3	1.12625	1.126254
		0.5	0.85391	0.853913
	0.1	0	1.77443	1.774455
		0.3	1.40123	1.401256
		0.5	1.06945	1.069473

The significant effect of the ferrofluid can only occur when there is an applied magnetic field. In this ferrofluid problem, we wanted to reveal the impact of the magnetic field when the Stefan blowing is present for the stretching/shrinking surface. Figure 2 shows the variations of the dimensionless wall shear stress, $C_f Re_x^{1/2}$, with the stretching/shrinking parameter, λ , for different magnetic interaction parameter, M , and the Stefan blowing parameter, κ , when other parameters were set as $\phi = 0.01$, $A = 1$, and $\delta = 1$. One can see that there exist second solutions for specific values of λ in the figure. Evidently, samples of the velocity profiles with second solutions are presented in Figure 3. Hence, we performed the stability analysis, and the smallest eigenvalues for the first and second solutions of some selected parameters are depicted in Table 4. It is seen that the first solutions have the smallest eigenvalues consisting of positive values, but the second solutions have negative eigenvalues. Thus, the first solutions are stable, while the second solutions are not stable. Due to the second solutions' unstable state, the discussions are limited to the behaviours portrayed by the first solution.

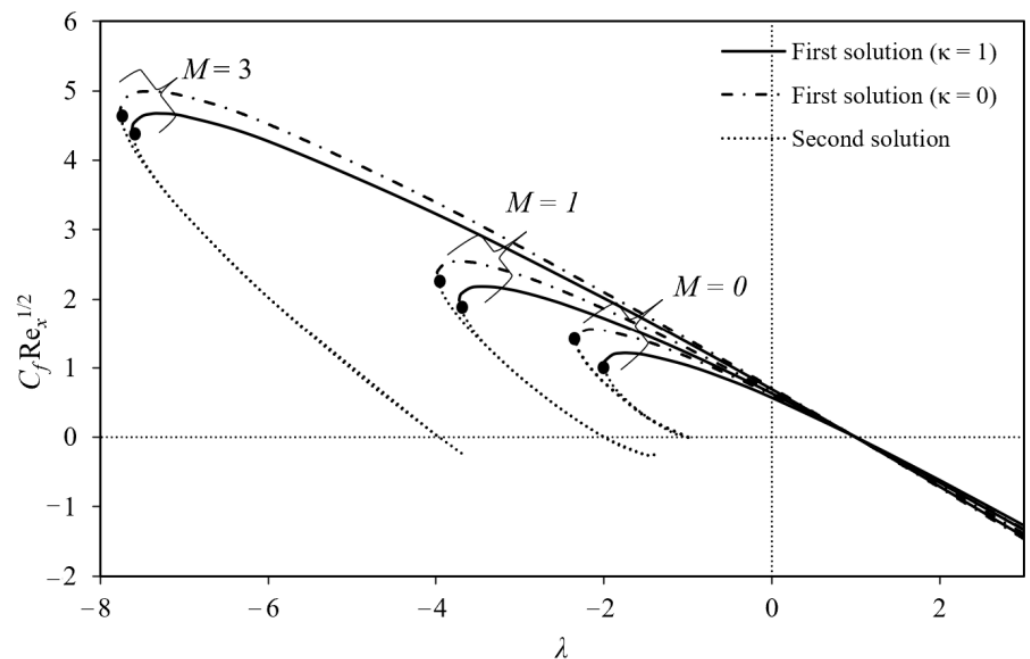


Figure 2. The variations of $C_f Re_x^{1/2}$ with the stretching/shrinking parameter, λ , for different M and κ when $\phi = 0.01$, $A = 1$, and $\delta = 1$.

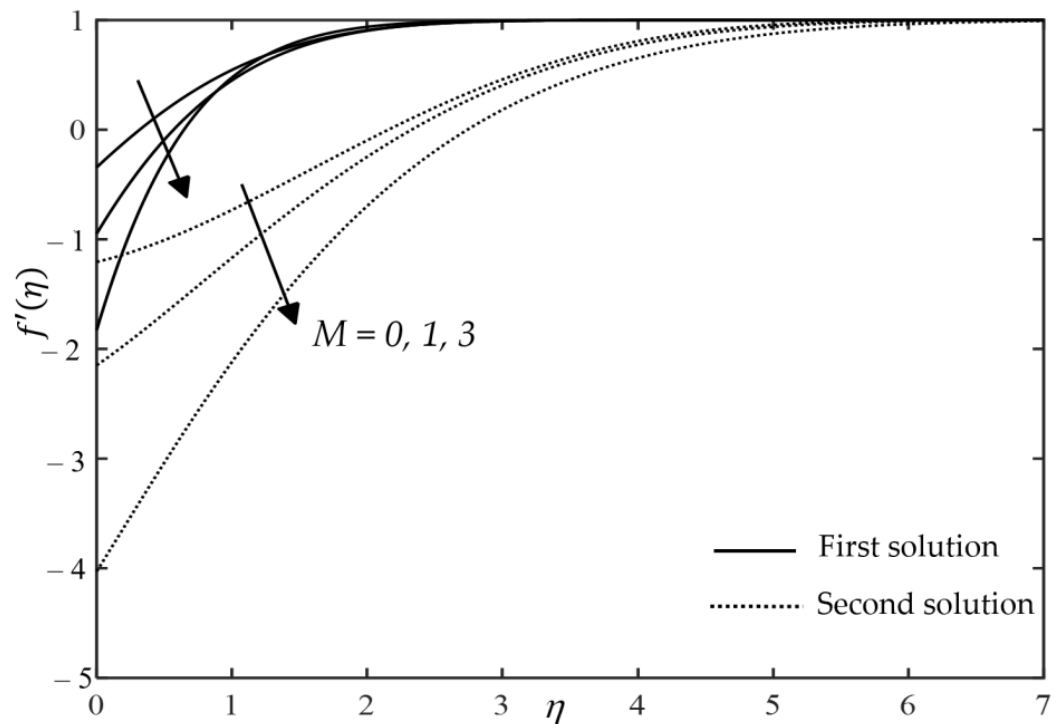


Figure 3. Velocity profiles for different M when $\phi = 0.01$, $A = 1$, $\kappa = 1$, and $\delta = 1$.

Table 4. Values of the smallest eigenvalues.

M	κ	λ	First Solution	Second Solution
0	0	-2	1.1610	-1.0347
		-2.3	0.3960	-0.3818
		-2.34	0.0607	-0.0603
	1	-1.8	0.8498	-1.0356
		-2	0.1383	-0.2353
		-2.006	0.0062	-0.0953
1	0	-3	2.1402	-1.8271
		-3.9	0.6383	-0.6135
		-3.98	0.2077	-0.2051
	1	-3	1.7442	-1.8234
		-3.7	0.4017	-0.5282
		-3.72	0.4011	-0.2867

Furthermore, it is also evident in Figure 2 that there is no wall shear stress when $\lambda = 1$, which indicates the ferrofluid moves at the same speed as the sheet. For $\lambda < 1$, all the values of $C_f Re_x^{1/2}$ are positive, inferring that ferrofluid exerts the drag towards the surface. In the region $\lambda > 1$, the values of $C_f Re_x^{1/2}$ are negative, indicating that the sheet’s surface exerts the drag force on the ferrofluid. Moreover, Figure 2 also reveals that the increment in M increases the critical points’ positions, wherein physically elucidating that boundary layer separation has been delayed. This observation is tally with the finding reported by Khan et al. [37]. This behaviour can be explained further where the magnetic field in the flow regime helps to sustain the kinetic energy of the fluid molecules, while preventing them from becoming drained. Conversely, Figure 2 shows that the increased influence of κ accelerates the boundary layer separation in the flow regime. The increased effect of κ depletes the fluid molecules’ kinetic energy and, hence, contributes to the earlier boundary layer separation event.

To see more precise effects of the parameters in the region $\lambda > 1$, Figure 4 is plotted. In Figures 2 and 4, we can see that the magnetic interaction parameter, M , increases the magnitudes of $C_f Re_x^{1/2}$ and broadens the range of solutions in the region $\lambda < 1$. On the other hand, the Stefan blowing parameter, κ , gives the opposite effect, i.e., decreases the magnitudes of $C_f Re_x^{1/2}$ and reduces the range of solutions in the region $\lambda < 1$. It is also noticed that parameter M lessens the momentum boundary layer thickness, while the parameter κ gives the opposite effect, as shown in Figure 5. A possible explanation for these results may be that the applied magnetic field produced a Lorenz force that opposed the flows towards the surface and compressed the boundary layer. However, the increase in the Stefan blowing means that extra motion in the ferrofluid produced by the diffusion of the species increases the boundary layer thickness. The species are pushed away from the surface, and ultimately, the skin friction or the shear stress is reduced. On the other hand, Table 5 shows that increasing the volume fraction of the magnetite ferroparticles increases the wall shear stress even in the presence of the Stefan blowing over the shrinking sheet. The inclusion of more magnetite ferroparticles past the tightening state of the sheet causes the friction drag of the surface to be increased. Consequently, the momentum boundary layer becomes thinner and impacts the increased value of $C_f Re_x^{1/2}$. It is worth highlighting that the effect of the Stefan blowing becomes insignificant with the presence of more magnetite ferroparticles volume fraction in the flow regime over the shrinking surface.

Table 5. Values of $C_f Re_x^{1/2}$ for magnetite ferrofluid with variations of M , κ , and ϕ when $\lambda = -2$.

ϕ	$M=0$		$M=1$	
	$\kappa=0$	$\kappa=1$	$\kappa=0$	$\kappa=1$
0	1.496369	1.041150	1.810827	1.667498
0.01	1.544701	1.089054	1.861782	1.714116
0.05	1.744903	1.257814	2.079717	1.915632
0.1	2.016981	1.468133	2.390081	2.206845

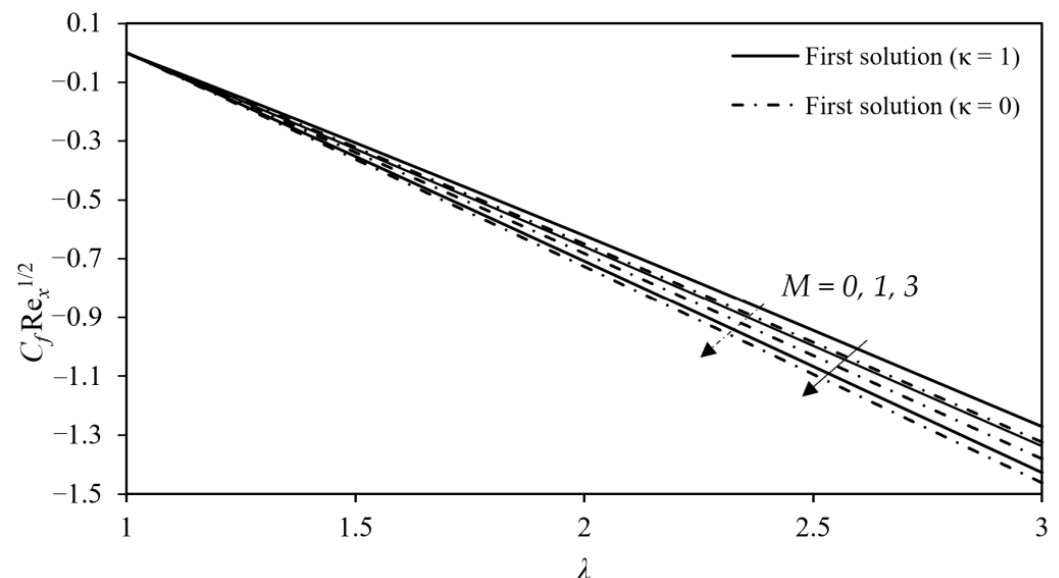


Figure 4. The behaviour of $C_f Re_x^{1/2}$ towards the stretching parameter, λ , for different M and κ when $\phi = 0.01$, $A = 1$, and $\delta = 1$.

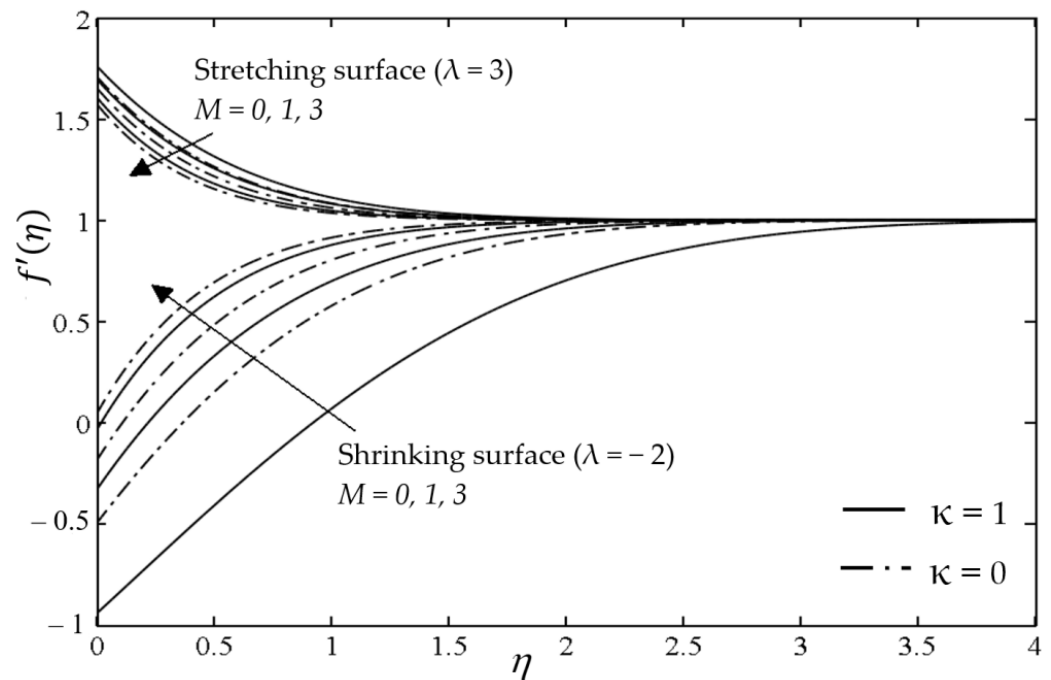


Figure 5. Impact of the magnetic parameter, M , on the velocity profiles for different κ and λ .

The dimensionless heat transfer coefficient, $Nu_x Re_x^{-1/2}$, trends concerning the stretching/shrinking parameter, λ , for different values of the magnetic interaction parameter, M , and the Stefan blowing parameter, κ , are shown in Figure 6. Figure 6 illustrates the heat transfer rate behaviour with and without the Stefan blowing effect. For the case that considers the Stefan blowing effect, the values of $Nu_x Re_x^{-1/2}$ increase with the increased effect of M . This can be explained from the aspect of species movement wherein the species also carry the heat while traveling, hence increasing the fluid temperature past the moving sheet. This essentially increased the surface heat flux and resulted in the enhanced values of $Nu_x Re_x^{-1/2}$. Alternatively, for the situation where the Stefan blowing effect is absent, $Nu_x Re_x^{-1/2}$ decreases when M intensifies. The diffusion of the species towards the ambient fluid may cause the deficiency of the ferrofluid on the surface and reduce the heat transfer rate past the moving sheet. Meanwhile, the effects of parameter M and parameter κ on the stretching/shrinking surface temperature profiles are displayed in Figure 7. These figures show that the heat transfer rate decreases, and the ferrofluid temperature distribution increases with the species Stefan blowing. The diffusion of the species towards the ambient fluid can cause the deficiency of the ferrofluid on the surface, reducing the rate of heat transfer. Another possible explanation is that the species also carry the heat while moving, consequently increasing the fluid temperature. In addition, Figures 6 and 7 also show that the magnetic interaction parameter, M , on the heat transfer coefficient and flow temperature is different in the regions $\lambda < 1$ and $\lambda > 1$. In the region $\lambda < 1$, the parameter M increases the heat transfer coefficient and reduces the temperature profiles. The opposite behaviour is observed in the region $\lambda > 1$. In this region, the ferrofluid flow slows down with the presence of a magnetic field. Consequently, this result produces a weaker convection and reduces the heat transfer. The present work infers that thermophoresis refers to the diffusion of the species particles saturated at the surface due to a temperature gradient. The effects of the thermophoresis or the Soret number parameter, S_T , on the velocity and the temperature profiles are presented in Figures 8 and 9, respectively. It is apparent from these figures that the effect of parameter S_T is significant on the velocity profiles and the temperature profiles only when the Stefan blowing is present. As illustrated in Figures 8 and 9, when the

parameter $\lambda > 1$, the Soret number reduces the velocity and temperature distribution. In contrast with the stretching sheet state, the Soret number increases the shrinking sheet's velocity and temperature distribution.

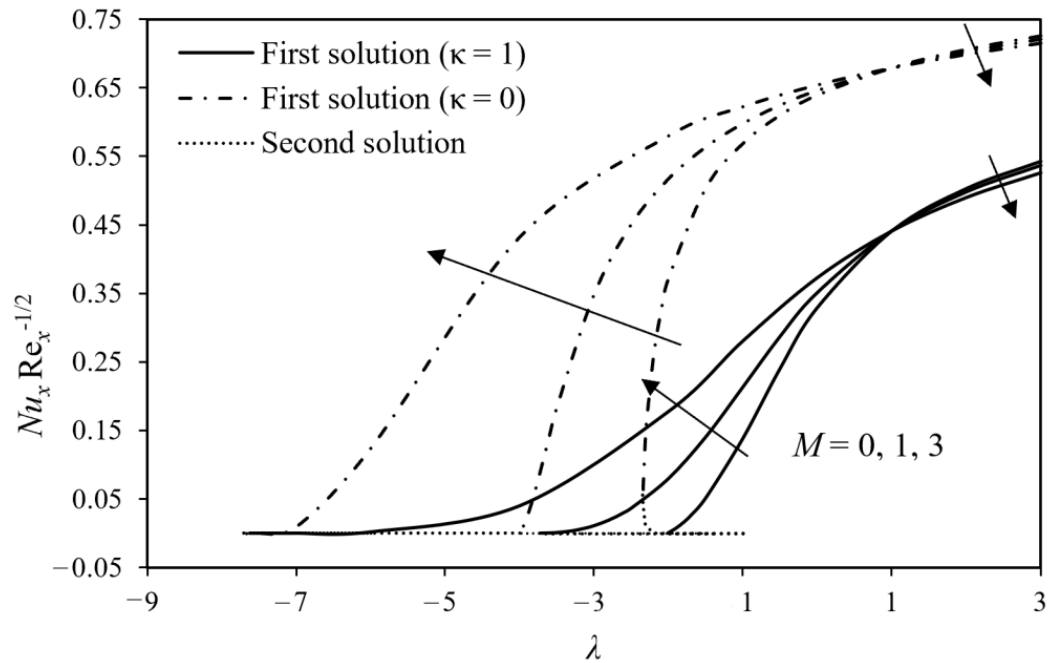


Figure 6. The variations of $Nu_x Re_x^{-1/2}$ with the stretching/shrinking parameter, λ , for different M and κ when $\phi = 0.01$, $A = 1$, and $\delta_T = 1$.

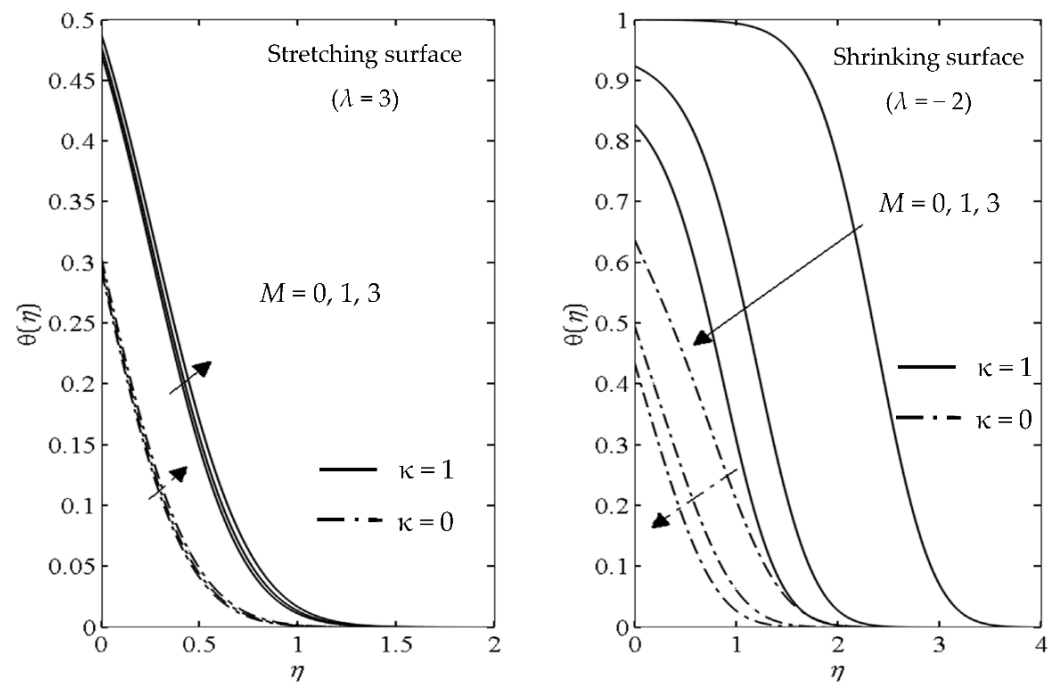


Figure 7. Effect of the magnetic interaction parameter, M , on the temperature profiles for different parameters κ and λ .

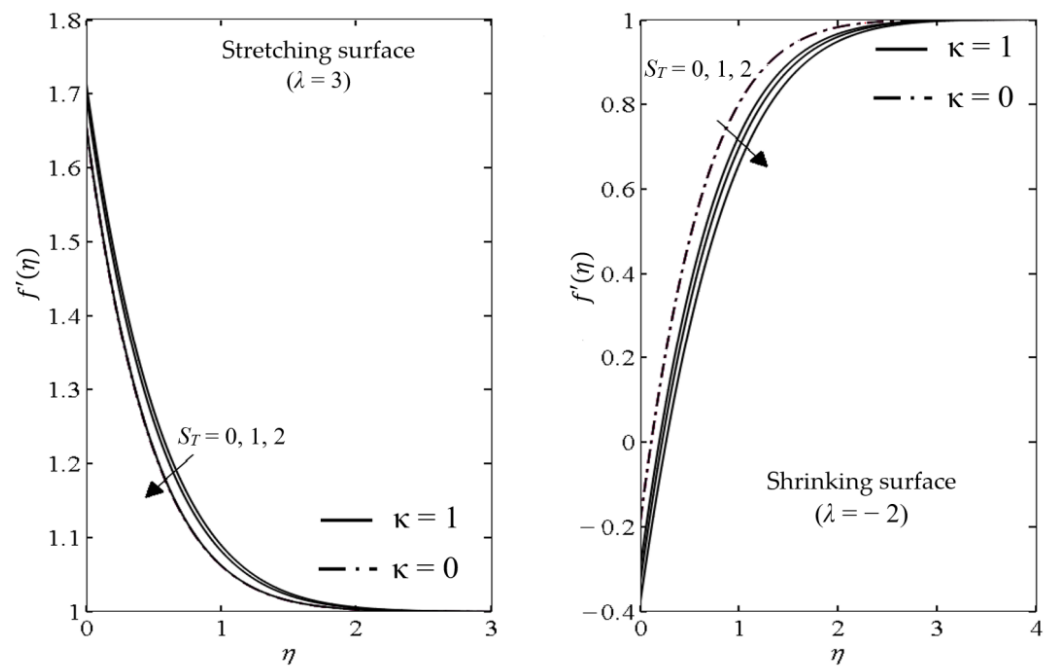


Figure 8. Influence of the Soret effect parameter, S_T , on the velocity profiles for different parameters κ and λ .

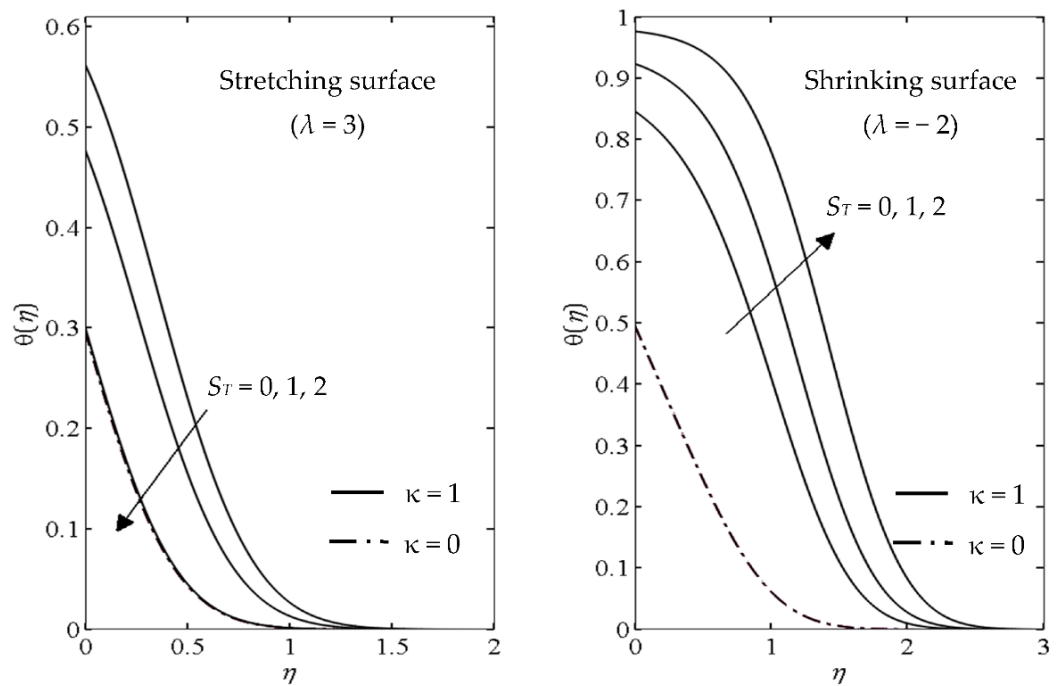


Figure 9. Influence of the Soret effect parameter, S_T , on the temperature profiles for different parameters κ and λ .

The flow with ultrafine particles is expected to experience a slip at the surfaces. Hence, the slip parameter was included, and the flow model is observed with the Stefan blowing effect. The impact of the velocity slip, δ , on the velocity profiles for different Stefan blowing intensities past the stretching/shrinking surfaces is depicted in Figure 10. For both surfaces, the velocity slip reduces the velocity distributions of the magnetite ferrofluid regardless of the Stefan blowing. Meanwhile, Figure 11 shows the effect of the thermal slip, δ_T , on the temperature profiles for the stretching and shrinking surfaces. Thermal slip has the effect of reducing the temperature distribution for both surfaces. The figure also shows that the temperature profiles are higher when the Stefan blowing is present. Lastly, we plotted the effects of the velocity ratio parameter, A , on the velocity and the temperature profiles as presented in Figures 12 and 13, respectively. The velocity ratio parameter is the ratio of the strength of the stagnation rates with the stretching/shrinking rates. In all the results above, we used $A = 1$, which means the strength of the stagnation flow and the stretching/shrinking flow are equal. As the parameter A increases, the strength of the stagnation flow probably exceeds the velocity of the stretching/shrinking flow and increases the acceleration of the external stream. Hence, we can see in Figure 12 that the velocity profiles will also increase for both surfaces. However, the thickness of the boundary layer reduces with parameter A , and a further reduction is noticed when the Stefan blowing is present for the stretching surface. Additionally, the thinning of the boundary layer thickness, as A increases, can be prevented when the Stefan blowing arises for the shrinking sheet. Furthermore, the parameter A reduces the temperature profiles, as shown in Figure 13. When the external stream of the stagnation velocity surpasses the stretching/shrinking velocity, the ferrofluid flow accelerates and produces a stronger thermal convection. This results in the increment of the heat transfer and reduces the temperature distribution.

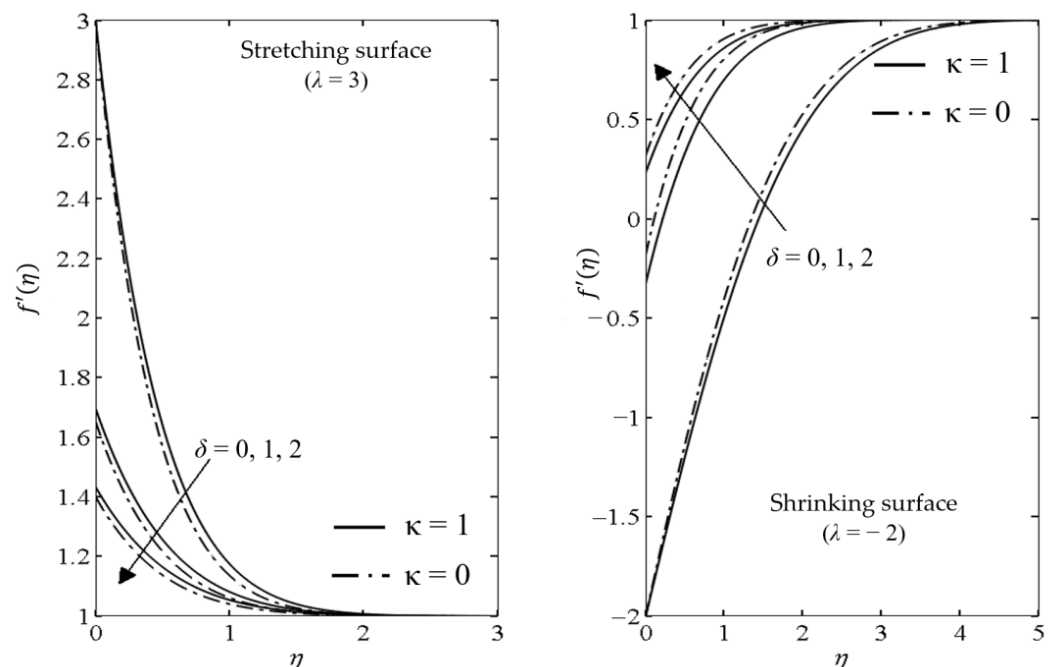


Figure 10. Effect of the velocity slip parameter, δ , on the velocity profiles for different parameters κ and λ .

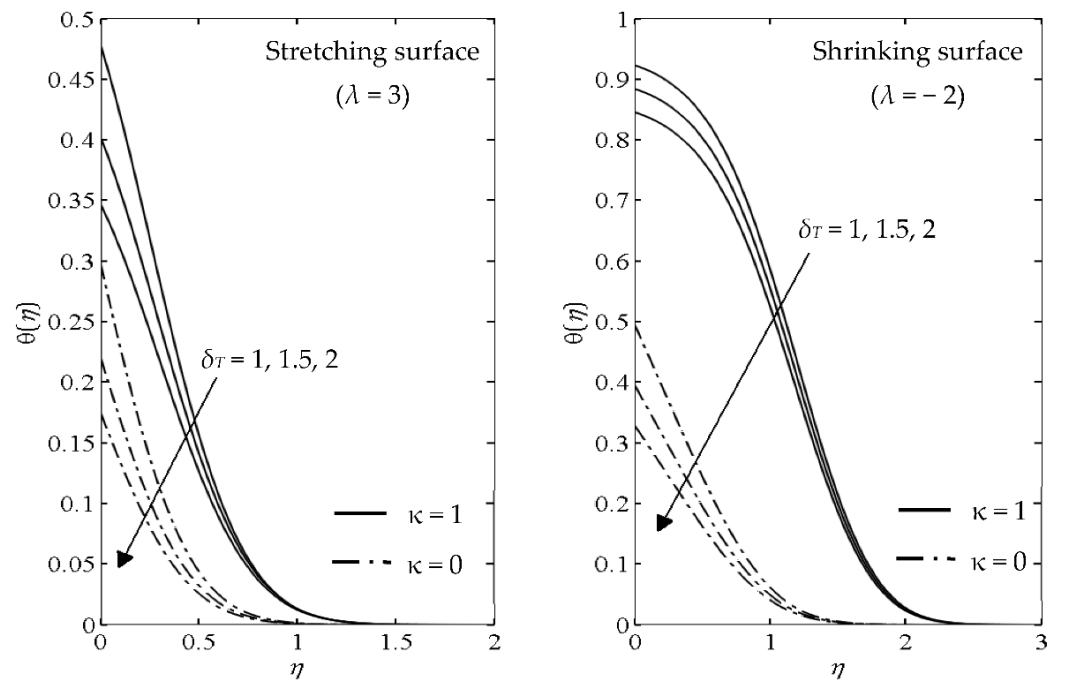


Figure 11. Effect of the thermal slip parameter, δ_T , on the temperature profiles for different parameters κ and λ .

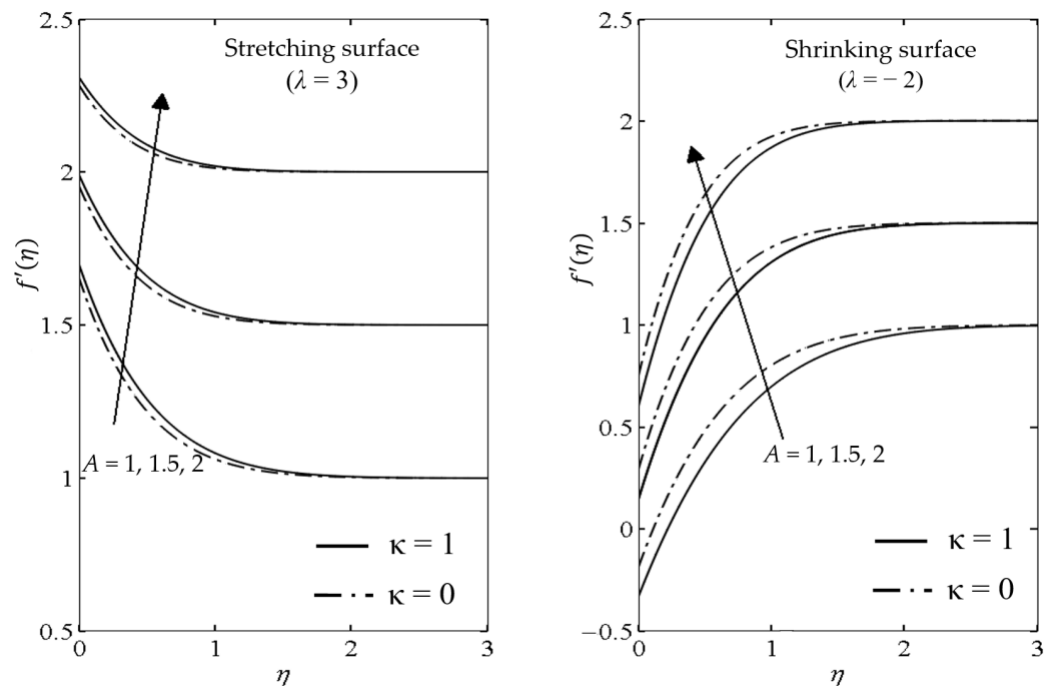


Figure 12. Effect of the velocity ratio parameter, A , on the velocity profiles for different parameters κ and λ .

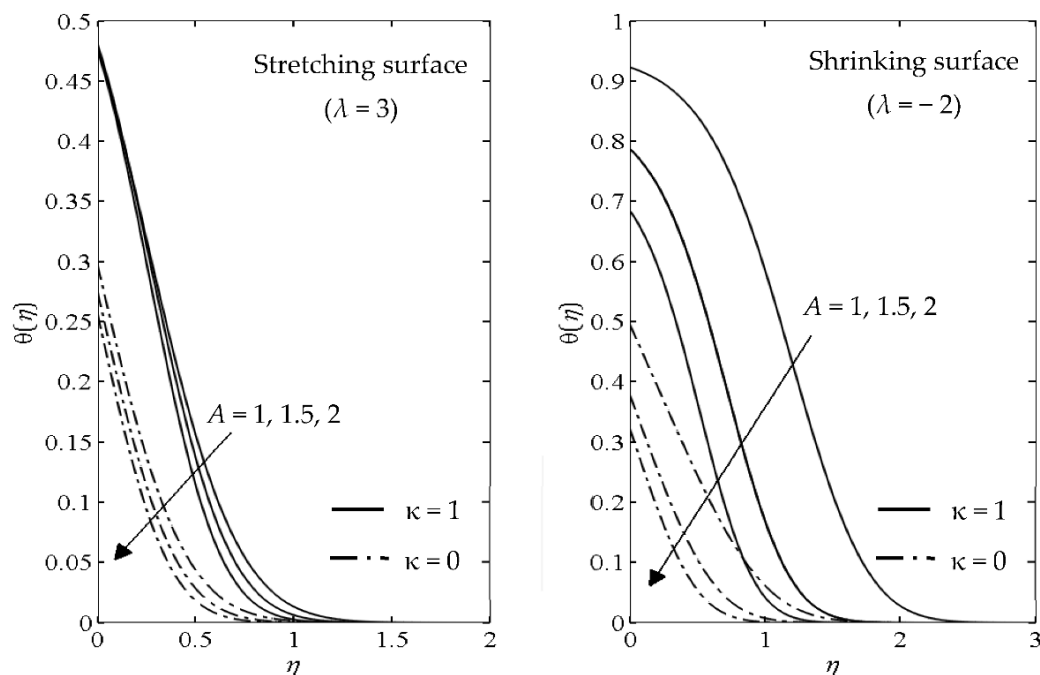


Figure 13. Effect of the velocity ratio parameter, A , on the temperature profiles for different parameters κ and λ .

5. Conclusions

The present theoretical work was devoted to examining upshots of the magnetic field, thermodiffusion, and slip on the magnetite ferrofluid flow when Stefan blowing is present. Overall, even though the increment in the magnetic field intensity in the flow regime increased the values of $C_f Re_x^{1/2}$ past the moving surface, it deferred the boundary layer separation in the ferrofluid. In contrast, the Stefan blowing effect expedited the boundary layer separation when its intensity was increased. Next, the present work found that the heat transfer rate augmented if and only if the presence of the Stefan blowing was true, and vice versa. The Soret number lowered the velocity and temperature distribution past the stretching sheet, and vice versa, for the shrinking state case. Further, the increment effect of the velocity slip lowered the velocity distributions of the magnetite ferrofluid irrespective of the Stefan blowing influence. The increment effect of the thermal slip decreased the temperature distribution, while the Stefan blowing promotes the temperature distribution in the flow regime. The increment impact of the velocity ratio parameter, A , heightened the velocity profiles, but lowered the temperature profiles past the moving surface. Additionally, the effects of the thermodiffusion and the slip were more noticeable if Stefan blowing existed at the surface. Finally, the second solution was found in this problem, and through a stability analysis, the solutions were confirmed to be unstable.

Author Contributions: Conceptualization, R.A.H. and I.P.; methodology, R.A.H.; software, R.A.H.; validation, I.P., R.N. and K.N.; formal analysis, R.A.H., K.N., R.N. and I.P.; investigation, R.A.H. and R.N.; writing—original draft preparation, R.A.H. and K.N.; writing—review and editing, K.N., R.N. and I.P.; visualisation, I.P.; supervision, R.N.; project administration, K.N.; funding acquisition, R.N. All authors have read and agreed to the published version of the manuscript.

Funding: This research was funded by the Universiti Kebangsaan Malaysia research grant (GUP-2019-034) and the Malaysia Ministry of Education, grant number FRGS/1/2020/STG06/UNIMAP/02/4.

Institutional Review Board Statement: Not applicable.

Informed Consent Statement: Not applicable.

Data Availability Statement: Not applicable.

Conflicts of Interest: The authors declare no conflict of interest. The funders had no role in the design of the study; in the collection, analyses, or interpretation of data; in the writing of the manuscript, or in the decision to publish the results.

References

1. Toledo, R.T. *Fundamentals of Food Process Engineering*; Springer: New York, NY, USA, 2007; pp. 413–429.
2. Ghosh, A.K. *Fundamentals of Paper Drying-Theory and Application from Industrial Perspective*; IntechOpen: Vienna, Austria, 2011; pp. 535–582.
3. Fang, T.; Jing, W. Flow, heat, and species transfer over a stretching plate considering coupled Stefan blowing effects from species transfer. *Commun. Nonlinear Sci. Numer. Simul.* **2014**, *19*, 3086–3097. [[CrossRef](#)]
4. Fang, T. Flow and mass transfer for an unsteady stagnation-point flow over a moving wall considering blowing effects. *J. Fluids Eng.* **2014**, *136*, 71103. [[CrossRef](#)]
5. Uddin, M.J.; Kabir, M.N.; Alginahi, Y.; Bég, O.A. Numerical solution of bio-nano-convection transport from a horizontal plate with blowing and multiple slip effects. *Proc. Inst. Mech. Eng. Part C J. Mech. Eng. Sci.* **2019**, *233*, 6910–6927. [[CrossRef](#)]
6. Zohra, F.T.; Uddin, M.J.; Basir, M.F.; Ismail, A.I.M. Magnetohydrodynamic bio-nano-convective slip flow with Stefan blowing effects over a rotating disc. *Proc. Inst. Mech. Eng. Part N J. Nanomater. Nanoeng. Nanosyst.* **2020**, *234*, 83–97.
7. Zohra, F.T.; Uddin, M.J.; Ismail, A.I.M.; Bég, O.A.; Kadir, A. Anisotropic slip magneto-bioconvection flow from a rotating cone to a nanofluid with Stefan blowing effects. *Chin. J. Phys.* **2018**, *56*, 432–448. [[CrossRef](#)]
8. Ryskin, A.; Pleiner, H. Influence of a magnetic field on the Soret-effect-dominated thermal convection in ferrofluids. *Phys. Rev. E* **2004**, *69*, 46301. [[CrossRef](#)]
9. Ramreddy, C.; Murthu, P.V.S.N.; Chamkha, A.J.; Rashad, A.M. Soret effect on mixed convection flow in a nanofluid under convective boundary condition. *Int. J. Heat Mass Transf.* **2013**, *64*, 384–392. [[CrossRef](#)]
10. Pal, D.; Mandal, G.; Vajravalu, K. Soret and Dufour effects on MHD convective-radiative heat and mass transfer of nanofluids over a vertical non-linear stretching/shrinking sheet. *Appl. Math. Comput.* **2016**, *287–288*, 184–200. [[CrossRef](#)]
11. Arif, U.; Nawaz, M.; Selmi, A.L. Numerical study of simultaneous transport of heat and mass transfer in Maxwell hybrid nanofluid in the presence of Soret and Dufour effects. *Phys. Scr.* **2022**, *97*, 025207. [[CrossRef](#)]
12. Uddin, M.J.; Kabir, M.N.; Bég, O.A. Computational investigation of Stefan blowing and multiple-slip effects on buoyancy-driven bioconvection nanofluid flow with microorganisms. *Int. J. Heat Mass Transf.* **2016**, *95*, 116–130. [[CrossRef](#)]
13. Singh, G.; Chamkha, A.J. Dual solutions for second-order slip flow and heat transfer on a vertical permeable shrinking sheet. *Ain Shams Eng. J.* **2013**, *4*, 911–917. [[CrossRef](#)]
14. Mahapatra, T.R.; Nandy, S.K. Slip effects on unsteady stagnation-point flow and heat transfer over a shrinking sheet. *Meccanica* **2013**, *48*, 1599–1606. [[CrossRef](#)]
15. Aman, F.; Ishak, A.; Pop, I. Magnetohydrodynamic stagnation-point flow towards a stretching/shrinking sheet with slip effects. *Int. Commun. Heat Mass Transf.* **2013**, *47*, 68–72. [[CrossRef](#)]
16. Merkin, J.H.; Lok, Y.Y.; Pop, I. A note on the stagnation-point flow over a permeable shrinking sheet with slip effects. *Int. Commun. Heat Mass Transf.* **2016**, *71*, 101–107. [[CrossRef](#)]
17. Wang, C.Y. Stagnation flow towards a shrinking sheet. *Int. J. Non. Linear. Mech.* **2008**, *43*, 377–382. [[CrossRef](#)]
18. Song, Y.Q.; Obideyi, B.D.; Shah, N.A.; Animasaun, I.L.; Mahrous, Y.M.; Chung, J.D. Significance of haphazard motion and thermal migration of alumina and copper nanoparticles across the dynamics of water and ethylene glycol on a convectively heated surface. *Case Stud. Therm. Eng.* **2021**, *26*, 101050. [[CrossRef](#)]
19. Liu, H.; Animasaun, I.L.; Shah, N.A.; Koriko, O.K.; Mahanthesh, B. Further discussion on the significance of quartic autocatalysis on the dynamics of water conveying 47 nm alumina and 29 nm cupric nanoparticles. *Arab J. Sci. Eng.* **2020**, *45*, 5977–6004. [[CrossRef](#)]
20. Elnaqeeb, T.; Animasaun, I.L.; Shah, N.A. Ternary-hybrid nanofluids: Significance of suction and dual-stretching on three-dimensional flow of water conveying nanoparticles with various shapes and densities. *Z. Naturforsch. A* **2021**, *76*, 231–243. [[CrossRef](#)]
21. Animasaun, I.L.; Shah, N.A.; Wakif, A.; Mahanthesh, B.; Sivaraj, R.; Koriko, O.K. *Ratio of Momentum Diffusivity to Thermal Diffusivity: Introduction, Meta-Analysis, and Scrutinization*, 1st ed.; Chapman and Hall: London, UK; CRC: London, UK, 2022.
22. Scherer, C.; Neto, A.M.F. Ferrofluids: Properties and applications. *Brazillian J. Phys.* **2005**, *35*, 718–727. [[CrossRef](#)]
23. Shokrollahi, H. Structure, synthetic methods, magnetic properties and biomedical applications of ferrofluids. *Mater. Sci. Eng. C* **2013**, *33*, 2476–2487. [[CrossRef](#)]
24. Ryskin, A.; Müller, H.W.; Pleiner, H. Thermodiffusion effects in convection of ferrofluids. *Magnetohydrodynamics* **2003**, *39*, 51–55.
25. Hayat, T.; Qayyum, S.; Imtiaz, M.; Alzahrani, F.; Alsaedi, A. Partial slip effect in flow of magnetite-Fe₃O₄ nanoparticles between rotating stretchable disks. *J. Magn. Magn. Mater.* **2016**, *413*, 39–48. [[CrossRef](#)]
26. Imtiaz, M.; Hayat, T.; Alsaedi, A. Convective flow of ferrofluid due to a curved stretching surface with homogeneous-heterogeneous reactions. *Powder Technol.* **2017**, *310*, 154–162. [[CrossRef](#)]

27. Rashad, A.M. Impact of thermal radiation on MHD slip flow of a ferrofluid over a non-isothermal wedge. *J. Magn. Magn. Mater.* **2017**, *422*, 25–31. [[CrossRef](#)]
28. Abbas, Z.; Sheikh, M. Numerical study of homogeneous-heterogeneous reactions on stagnation point flow of ferrofluid with non-linear slip condition. *Chin. J. Chem. Eng.* **2017**, *25*, 11–17. [[CrossRef](#)]
29. Hamid, R.A.; Nazar, R.; Naganthran, K.; Pop, I. Dusty ferrofluid transport phenomena towards a non-isothermal moving surface with viscous dissipation. *Chin. J. Phys.* **2022**, *75*, 139–151. [[CrossRef](#)]
30. Khan, Z.H.; Khan, W.A.; Qasim, M.; Shah, I.A. MHD stagnation point ferrofluid flow and heat transfer toward a stretching sheet. *IEEE Trans. Nanotechnol.* **2014**, *13*, 35–40. [[CrossRef](#)]
31. Rosca, N.S.; Rosca, A.V.; Merkin, J.H.; Pop, I. Mixed convection flow, heat transfer, species concentration near the stagnation point on a vertical plate with Stefan coupled blowing. *Int. J. Numer. Methods Heat Fluid Flow* **2017**, *27*, 77–103. [[CrossRef](#)]
32. Rashad, A.M. Impact of anisotropic slip on transient three dimensional MHD flow of ferrofluid over an inclined radiate stretching surface. *J. Egypt. Math. Soc.* **2017**, *25*, 230–237. [[CrossRef](#)]
33. Zainal, N.A.; Nazar, R.; Naganthran, K.; Pop, I. Stability analysis of unsteady MHD rear stagnation point flow of hybrid nanofluid. *Mathematics* **2021**, *9*, 2428. [[CrossRef](#)]
34. Merkin, J.H. Mixed convection boundary layer flow on a vertical surface in a saturated porous medium. *J. Eng. Math.* **1980**, *14*, 301–313. [[CrossRef](#)]
35. Sheikholeslami, M.; Ganji, D.D. Nanofluid convective heat transfer using semi analytical and numerical approaches: A review. *J. Taiwan Inst. Chem. Eng.* **2016**, *65*, 43–77. [[CrossRef](#)]
36. Mahapatra, T.R.; Gupta, A.S. Heat transfer in stagnation-point flow towards a stretching sheet. *Heat Mass Transf.* **2002**, *38*, 517–521. [[CrossRef](#)]
37. Khan, U.; Waini, I.; Zaib, A.; Ishak, A.; Pop, I. MHD mixed convection hybrid nanofluids flow over a permeable moving inclined flat plate in the presence of thermophoretic and radiative heat flux effects. *Mathematics* **2022**, *10*, 1164. [[CrossRef](#)]